Cellulose-Nanowhisker-Templated Synthesis of Titanium Dioxide/Cellulose Nanomaterials with Promising Photocatalytic Abilities

Shilin Liu, Dandan Tao, Huiyu Bai, Xiaoya Liu

College of Chemical and Material Engineering, Jiangnan University, Wuxi, Jiangsu 214122, China

Received 12 July 2010; accepted 28 November 2011
DOI 10.1002/app.36637
Published online in Wiley Online Library (wileyonlinelibrary.com).

ABSTRACT: By using native cellulose nanowhiskers as green templates, we prepared TiO_2/cellulose nanomaterials via a sol–gel process from the hydrolysis of $Ti(OC_2H_5)_4$. The structures and properties of the composite nanoparticles were characterized with X-ray diffraction, transmission electron microscopy, thermogravimetric analysis, ultraviolet–visible spectroscopy, and photocatalytic degradation tests. The TiO_2/cellulose nanoparticles with low loadings of TiO_2 nanoparticles exhibited obvious quantum size effects and lower band gaps. The composite nanoparticles had promising photocatalytic activity for the photodegradation of a methyl orange solution under weak UV light irradiation. Furthermore, they exhibited good stability against photocorrosion, so it is possible that they could be used in the photodegradation of organic pollutants. © 2012 Wiley Periodicals, Inc. J Appl Polym Sci 000: 000–000, 2012

Key words: biomaterials; biomineralization; nanocomposites; nanoparticle; nanotechnology

INTRODUCTION

Titanium dioxide (TiO_2), with its two common crystal forms (rutile and anatase), is an important semiconductor material. The rutile phase of TiO_2 has a high refractive index and is often used in optical devices such as waveguides.[1] Anatase TiO_2 has photocatalytic activity and is widely applied in photocatalysts,[2,3] solar energy cells,[4–6] antibacterials,[7] gas sensors,[8] catalyst supports,[9] and pigments.[10] These applications are often dependent on the particle size, morphology, phase, and crystallinity of the particles. The ability to prepare size- and shape-controlled nanocrystals enables these crystals to be used as key components for the fabrication of advanced nanodevices. Nanocrystals with tailored shapes have attracted extensive interest in the past decade because of their many intrinsic shape-dependent properties. Many reports have described the shape-controlled synthesis of TiO_2 nanocrystals, such as through the sol–gel process,[11] surfactant-directed method,[12–14] hydrothermal technique,[15] solvothermal method,[16] chemical vapor deposition,[17] and reverse micelle method.[18] Among these methods, the solvothermal method normally has a better ability to control the size and shape distributions of the TiO_2 nanocrystals because a great variety of organic solvents can be chosen.[19–21] Unfortunately, most organics are toxic and highly reactive chemicals and may pose potential environmental and biological risks. Anodic aluminum oxide membranes[22–25] or diblock polymers[26] are also novel candidates for the templated preparation of TiO_2 nanomaterials with controlled morphology, but the templates used thus far have not been cost effective, and they have often been prepared in a multistep approach. Therefore, from a green chemistry perspective, it is highly desirable to develop a simple and low-cost method for the preparation of TiO_2 nanomaterials.

Cellulose whiskers, which are prepared from the hydrolysis of native cellulose, are gaining momentum recently because of their combination of natural and renewable origins and their equally impressive mechanical properties compared with carbon nanotubes.[27] It is inherently a low-cost material and is available from a variety of natural sources, such as cotton,[28] tunicates,[29] algae,[30] bacteria,[31] and wood.[32] Depending on its source, cellulose whiskers are also available in a wide variety of aspect ratios (e.g., $\sim$ 200 nm long and 5 nm in lateral dimension and up to several micrometers long and 15 nm in lateral dimension). In our previous works, we paid an extensive amount of attention to the preparation of

Correspondence to: S. Liu (slliu2009@jiangnan.edu.cn) or X. Liu (lxy@jiangnan.edu.cn).

Contract grant sponsor: National Natural Science Foundation of China; contract grant number: 51003043.
Contract grant sponsor: Jiangnan University; contract grant number: JUSRP11107.

cellulose-based nanocomposites by the *in situ* synthesis of inorganic nanoparticles in porous structured regenerated cellulose materials,[33–38] and pure inorganic nanomaterials with high surface areas and transnormal properties were also prepared successfully with regenerated cellulose fibers as templates.[39] It is interesting that native cellulose whiskers also can be used as templates for the preparation of functional inorganic nanomaterials. Compared with the conventional inorganic or organic templates that are used for the preparation of nanomaterials, cellulose whiskers are easier to get and cheaper, and their most important virtue is their regenerative and environmental friendly nature and easy removability. In this study, we prepared one-dimensional TiO_2 nanomaterials by using natural cellulose whiskers as templates, and the effects of the hydrolysis conditions on the morphology and size of the cellulose whiskers and on the properties of TiO_2/cellulose nanoparticles were investigated. We hoped to provide a facile method for preparing TiO_2/cellulose photocatalysts. This may also provide a new and "green" pathway for the routine design and fabrication of other functional nanomaterials and open new application ranges for cellulose.

EXPERIMENTAL

Chemicals

Native cellulose [cotton linter, α-cellulose ≥ 95%, viscosity-average molecular weights (M_η) = 1.07×10^5 in cadoxen at 25°C] was supplied by Hubei Chemical Fiber Co., Ltd. (Xiangfan, Hubei, China). Other analytical-grade chemical reagents were supplied by Sinopharm Chemical Reagent Co., Ltd. (Shanghai, China) and were used without further purification.

Preparation of the cellulose nanowhiskers

The cellulose nanowhiskers were prepared by the hydrolysis of cotton linter with sulfuric acid. Briefly, 5 g of the cotton linter powder was mixed with 87.5 mL of 64% (w/v) sulfuric acid and stirred at 45°C for different times. The suspension was diluted fivefold with deionized water, then centrifuged, and washed with water three times. The precipitate was dialyzed against deionized water until the pH became neutral and was then freeze-dried. The cellulose nanowhiskers prepared for hydrolysis times of 1, 2, 3, and 4 h were coded as CW-1, CW-2, CW-3, and CW-4, respectively.

Preparation of the TiO_2/cellulose nanomaterials

Cellulose nanowhiskers (0.2 g), HNO_3 (5 mL, 0.1*M*), and absolute ethanol (100 mL) were mixed with each other in a round flask, and the mixed suspension was ultrasonically dispersed for 1 h. Subsequently, 1 mL of titanium(IV) ethoxide [$Ti(OC_2H_5)_4$ or TEOT] was added to this mixture slowly with a constant pressure funnel under magnetic stirring. The reaction temperature was kept at 40 ± 0.2°C for 4 h. Finally, the suspension was diluted fivefold with water, then centrifuged, and washed with water repeatedly. The precipitate was dialyzed against deionized water for 2 days and then freeze-dried. The TiO_2/cellulose nanoparticles prepared from CW-1, CW-2, CW-3, and CW-4 were coded as CWT-1, CWT-2, CWT-3, and CWT-4, respectively.

Photocatalytic degradation of methyl orange (MO)

We assessed the photocatalytic activities of the TiO_2/cellulose nanoparticles monitoring the degradation of MO. TiO_2/cellulose nanoparticles (40 mg) were mixed with 110 mL of aqueous MO solution (1.92×10^{-4} mol/L) in the dark for 30 min to obtain the saturated adsorption of MO before UV light irradiation. Then, the solution with the TiO_2/cellulose nanoparticles was irradiated under UV light. The mean light intensity of the UV light was about 0.315 W/cm^2, and the irradiation surface area was about 78.5 cm^2. The concentration of MO was monitored by the detection of its UV absorbance intensity at 464 nm at given irradiation time intervals. A blank experiment was also carried out under the same conditions with pristine cellulose nanowhiskers. To investigate the influence of the UV intensity on the photocatalytic performance of the TiO_2/cellulose nanoparticles, the CWT-4 sample with a weight of 20 mg was used in tests with the same method.

Characterization

Wide-angle X-ray diffraction (XRD) measurement was carried out on an XRD diffractometer (D8-Advance, Bruker). The patterns with Cu Kα radiation (weighted-average λ = 0.15406 nm) at 40 kV and 40 mA were recorded in the region of 2θ from 8 to 70°, with a step speed of 1°/min. Thermogravimetric analysis was carried out with a thermogravimetric analyzer (Ulvac TGD 9600, Japan). The sample was placed in a platinum pan and heated from 20 to 700°C at a rate of 10 K/min in an air atmosphere. A nitrogen adsorption–desorption test was performed with a Quantachrome NOVA 4200e (Quantachrome, USA), and Brunauer–Emmett–Teller (BET) analysis was performed with the Autosorb program (Quantachrome) with a relative vapor pressure of 0.05–0.3 at 77 K. Transmission electron microscopy (TEM) was carried out on a JEOL-1010 (Japan) electron microscope at an accelerating voltage of 200 kV. Ultraviolet–visible (UV–vis) spectroscopy

measurement was carried out on a UV–vis spectroscope (UV-160A, Shimadzu, Japan).

RESULTS AND DISCUSSION

Structure and properties of the cellulose nanowhiskers

Figure 1 shows TEM images of the cellulose nanowhiskers that were isolated from the cotton linter by acid hydrolysis. The cellulose nanowhiskers had a rodlike morphology, lengths of 12–20 nm, and widths of 4–6 nm. The length of the cellulose nanowhiskers was measured directly from TEM images, and the width was defined as the largest dimension measured along the nanoparticle perpendicular to its long axis. The corresponding aspect ratio (length/width) histograms of the cellulose nanowhiskers prepared for different hydrolysis times are also shown in Figure 1. With an increase in the hydrolysis time, the fraction of shorter particles increased, and no clear trend was observed in the width. Therefore, the aspect ratio (length/width) decreased from 4 to 2.75. When native cellulose was treated with sulfuric acid, disordered or paracrystalline regions were preferentially hydrolyzed, whereas crystalline regions that had a higher resistance to acid attack remained intact. After the acid treatment, which led to the removal of the microfibrils at the defects, the cellulose nanowhiskers were obtained.[40] The actual occurrence of the size and aspect ratio of the cellulose nanowhiskers decreased with increasing hydrolysis time was attributed to the kinetics of acid hydrolysis, and it was discussed in detail earlier.[31] The results indicate that the size and morphology of the cellulose nanowhiskers could be controlled by changes in the hydrolysis conditions. This would be attractive for the preparation of nanomaterials from native cellulose, for the particle sizes and morphologies of the synthesized inorganics could be controlled by changes in that of the used templates.

The nitrogen adsorption/desorption isotherms of the cellulose nanowhiskers are shown in Figure 2. There were considerably broadened hysteresis loops for all the samples, and the loops did not level off at relative pressures close to the saturation vapor pressure. According to IUPAC, it could be classified as a type of H_3 hysteresis; this suggests that the nanoparticles were composed of aggregates (loose assemblages).[41] Because of the strong interactions between the cellulose nanowhiskers, the nanoparticles tended to attract each other and form loose assemblages but not monolithic ones. The observed broadening of the hysteresis loop most likely arose from the lack of uniformity of pore diameter between the nanowhiskers. During desorption, narrower pore parts, which still contained condensed nitrogen, prevented capillary evaporation from wider parts of the pores,[42] and the pore connectivity effects were an additional cause of the observed broadening of the hysteresis loop.[43] The BET surface areas of the cellulose nanowhiskers are shown in Figure 2(b). With an increase in the hydrolysis time from 1 to 4 h, the BET surface areas of the nanowhiskers increased from 78 to 110 $m^2\ g^{-1}$. This indicated that the particle size of the cellulose nanowhisker decreased with increasing hydrolysis time. This further supported the conclusions obtained from TEM.

Structure of the TiO_2/cellulose nanomaterials

Cellulose is a multihydroxyl polymer. It may have reacted with the TiO_2 precursor during the hydrolysis of TEOT. Figure 3 shows the XRD of the cellulose nanowhiskers, and the cellulose nanowhiskers reacted with TEOT. The diffraction peaks at $2\theta = 14.8$, 16.3, 22.5, and 34.4° were for $(1\bar{1}1)$, (110), (200), and (044), respectively, of the cellulose nanowhiskers. These were typical of cellulose I.[44] In addition to the peaks of cellulose I, there were some other diffraction peaks at 2θ values of 25.5, 37.8, 48.3, 54.4, and 62.9°; these indicated that anatase TiO_2 (JCPDS (Joint Committee on Powder Diffraction Standards) card no: 21-1272) was formed on the surface of the cellulose nanowhiskers. The diffraction lines were relatively broad, which indicated that the nanosized TiO_2 had a high crystallinity,[45] and the particle sizes of the TiO_2 nanoparticles estimated from the width of the (101) diffraction peak with the Scherrer formula were about 3.41, 3.18, 3.31, and 3.59 nm for CWT-1, CWT-2, CWT-3, and CWT-4, respectively. There was no obvious difference in the particle size of the synthesized TiO_2 nanoparticles with the cellulose nanowhiskers as templates.

Figure 4 shows the TEM images of the TiO_2/cellulose nanoparticles. There was no obvious change in the morphologies of the nanoparticles compared with those of pristine cellulose nanowhiskers. It was worth noting that the aspect ratio (length/width) of the nanoparticles decreased from 3.0 to 2.0; this was a little smaller than that of the pristine cellulose nanowhiskers and was ascribed to the coating of the TiO_2 nanoparticles on the surface of the cellulose nanowhiskers. When the cellulose nanowhiskers were mixed with TEOT, the TiO_2 precursor molecules were quickly adsorbed and reacted with the functional groups (—OH) on the surface of the cellulose nanowhiskers. Water molecules subsequently were generated from the condensation reaction. This led to the tight anchoring of the molecules on the surface of host cellulose whiskers, which formed a uniform guest coating. According to the results of XRD, this indicated that the cellulose nanowhiskers could be used as templates for the synthesis of functional inorganic nanomaterials.

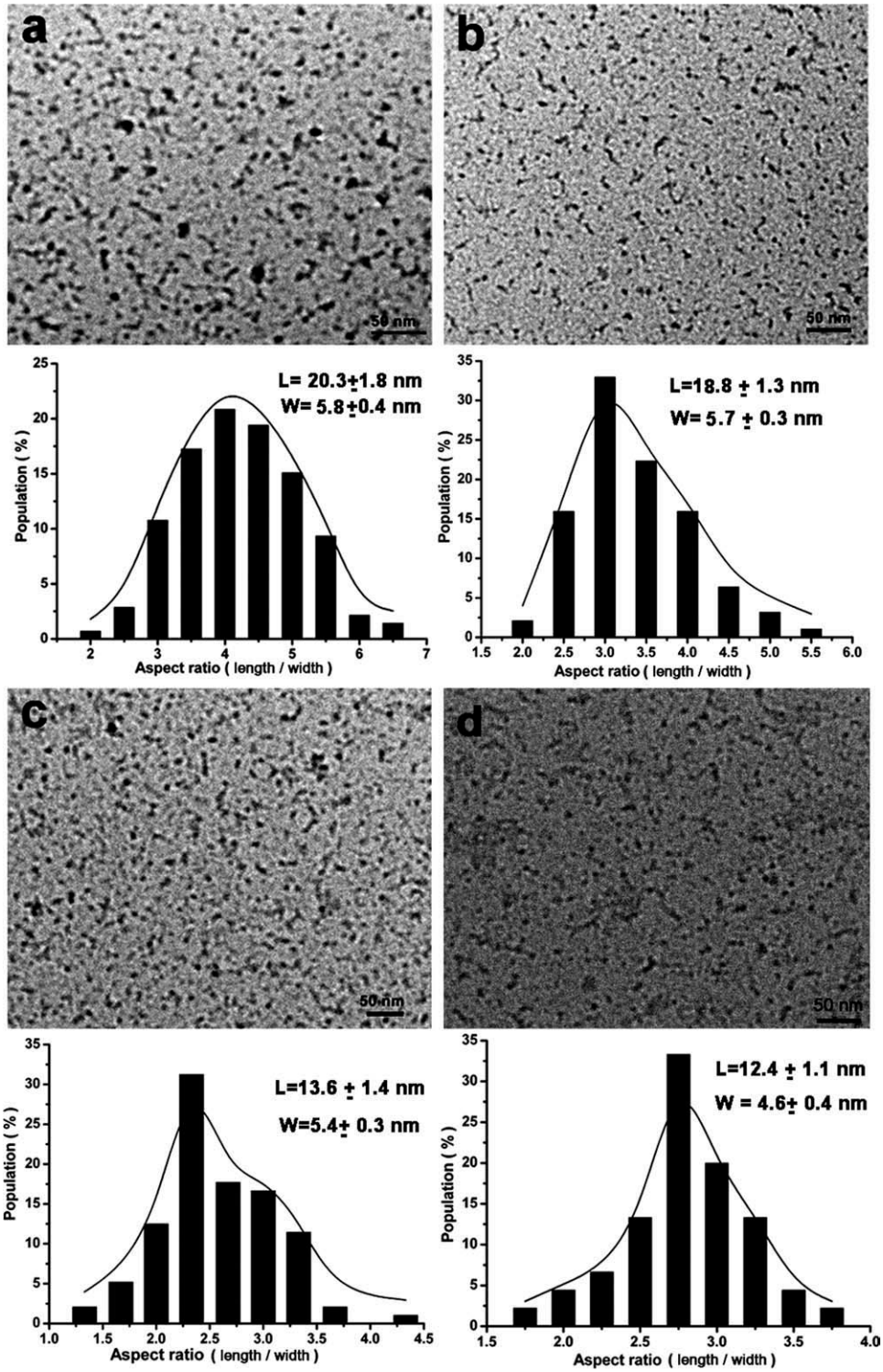

Figure 1 TEM images and statistical particle size distribution of the cellulose nanowhiskers prepared with different hydrolysis times: (a) CW-1, (b) CW-2, (c) CW-3, and (d) CW-4 (L = length; W = width; higher resolution for the TEM images were not available).

Thermal degradation patterns of the cellulose nanowhiskers and the TiO_2/cellulose nanoparticles are shown in Figure 5. A small weight loss of 8–11% around 80°C was assigned to the release of moisture from the samples. The pure cellulose nanowhiskers showed two obvious weight loss steps with increasing temperature. The first weight loss was found in the temperature range 300–380°C and was ascribed to the onset of cellulose decomposition. The second weight loss peak at 420–540°C was attributed to the decomposition and

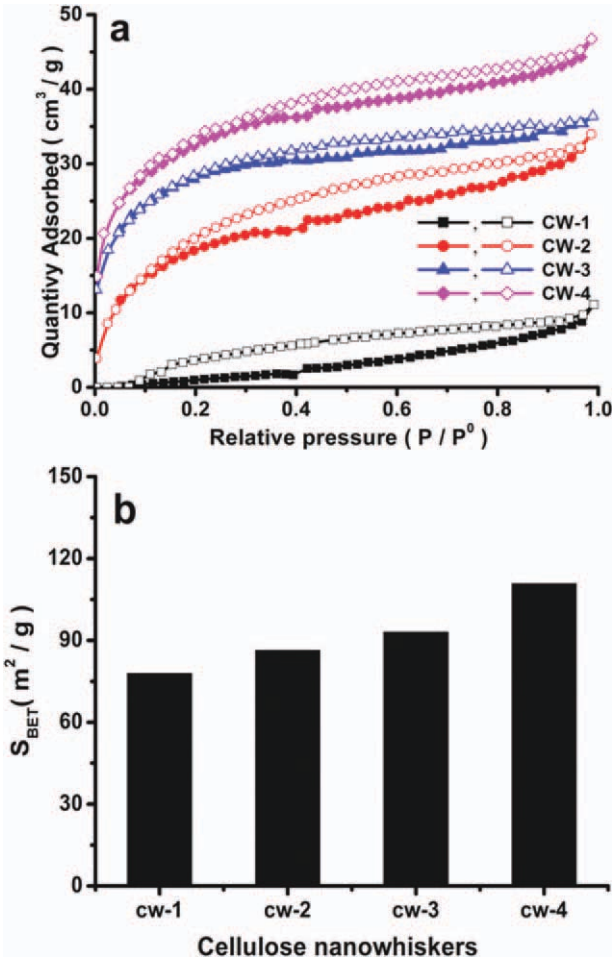

Figure 2 (a) Nitrogen gas adsorption–desorption isotherms and (b) corresponding BET surface areas (S_{BET}'s) of cellulose nanowhiskers prepared with different hydrolysis times (solid symbols indicate adsorption and open symbols indicate desorption). P, was the testing pressure, and P^o was the atmospheric pressure. [Color figure can be viewed in the online issue, which is available at wileyonlinelibrary.com.]

carbonization of cellulose. The native cellulose nanowhiskers decomposed at 353°C, whereas the onset decomposition temperature of the TiO_2/cellulose nanoparticles was higher than that of the pure cellulose nanowhiskers. This suggested that the flame retardancy of the cellulose improved by the incorporated TiO_2 coating and the higher content of TiO_2 coating contributed to a higher flame-retardant performance. It further indicated that TiO_2 was synthesized on the surface of the cellulose nanowhiskers. The contents of the thermal degradation residues of the TiO_2/cellulose nanoparticles were 42.37, 48.11, 49.35, and 50.60 wt % for CWT-1, CWT-2, CWT-3, and CWT-4, respectively. This suggested that the cellulose nanowhiskers had a high reactive ability with TEOT. The content of the coated TiO_2 on the cellulose nanowhiskers increased with increasing hydrolysis time. This resulted from the differences in the surface areas of the cellulose nanowhiskers.

Figure 6(a) shows the nitrogen adsorption/desorption isotherm of the TiO_2/cellulose nanoparticles. Interestingly, the hysteresis loops were obviously different from those of original cellulose nanowhiskers. It was classified as type H1 according to IUPAC; this indicated that the TiO_2/cellulose nanoparticles consisted of agglomerates (assemblages of rigidly joined particles) or compacts of approximately spherical particles arranged in a fairly uniform way.[46] It further suggested that the TiO_2 nanoparticles were synthesized on the surface of cellulose nanowhiskers. The BET surface area of the TiO_2/cellulose nanoparticles is shown in Figure 6(b). All of the composite nanowhiskers had larger specific surface areas than that of the corresponding pristine cellulose nanowhiskers. This indicated that the cellulose nanowhiskers used as templates had a significant influence on the surface morphology and surface area of the resulting composite nanoparticles. When the cellulose nanowhiskers were not coated with TiO_2 nanoparticles, they were prone to form aggregates compared with the TiO_2/cellulose nanoparticles, and the coating of TiO_2 nanoparticles on the surface of the cellulose nanowhiskers enhanced its dispersability. This is very important for the use of the nanomaterials.

Properties of the TiO_2/cellulose nanomaterials

Figure 7(a) shows the UV–vis absorption of the cellulose nanowhiskers and TiO_2/cellulose nanocomposites. The TiO_2/cellulose nanomaterials presented a typical band-to-band absorption in the visible spectral region because of the incorporated TiO_2 nanoparticles, whereas the cellulose nanowhiskers did not show obvious optical absorption in the same

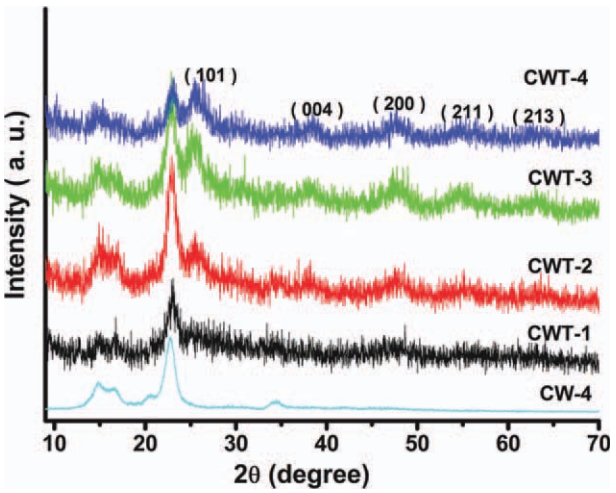

Figure 3 Powder XRD pattern of the cellulose nanowhiskers and TiO_2/cellulose nanoparticles. [Color figure can be viewed in the online issue, which is available at wileyonlinelibrary.com.]

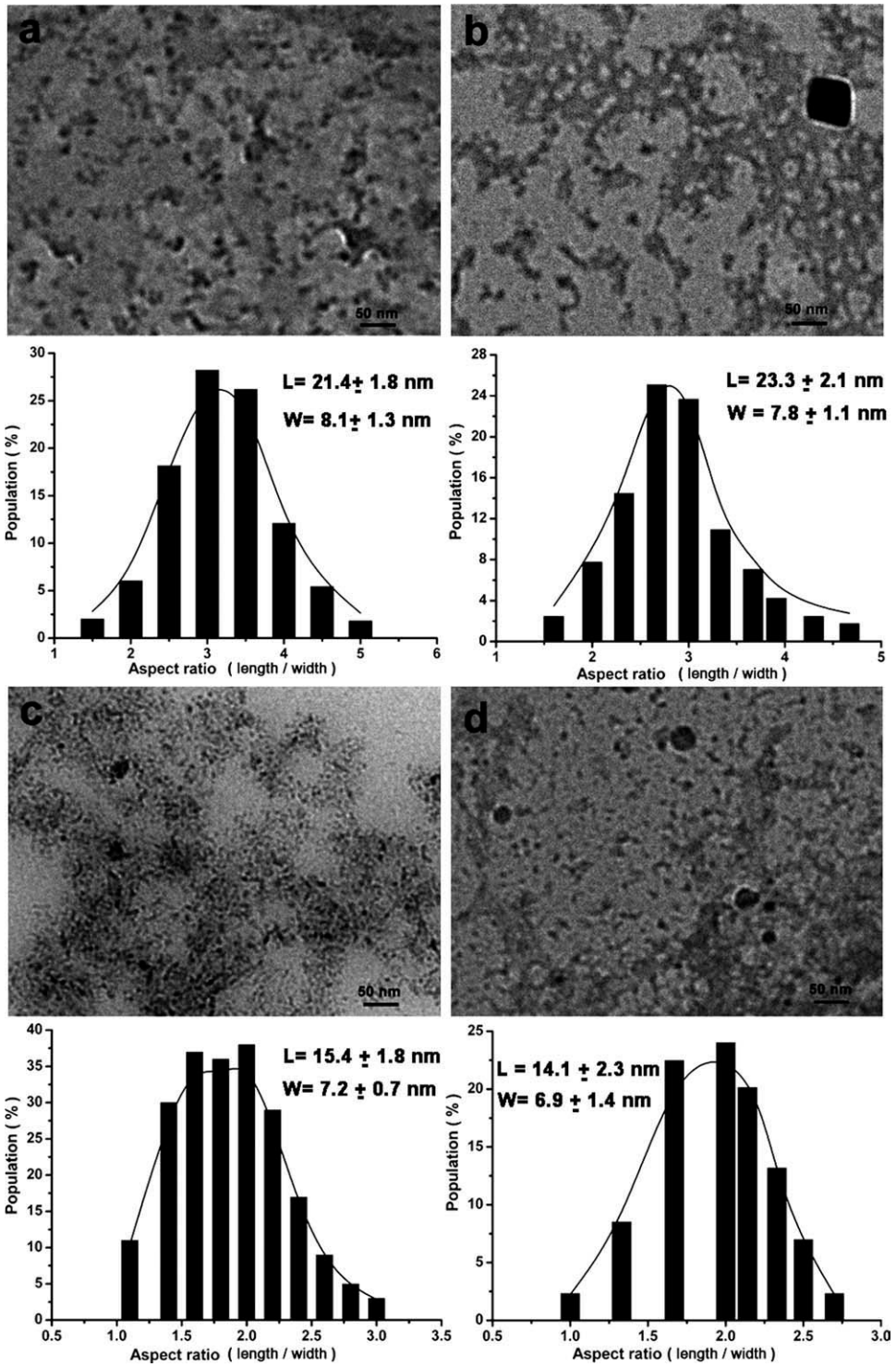

Figure 4 TEM images and statistical particle size distribution of the TiO_2/cellulose nanoparticles prepared from different cellulose nanowhiskers used as templates: (a) CWT-1, (b) CWT-2, (c) CWT-3, and (d) CWT-4 (L = length; W = width; higher resolution for the TEM images were not available).

spectral region. It was noteworthy that the absorption onset gradually shifted to a longer wavelength region with the loading of TiO_2 nanoparticles, and there were obvious redshifts compared to the band-gap absorption (330–350 nm) of bulk anatase TiO_2. Such a spectral shift could have been induced by the quantum size effect of the loaded semiconductor TiO_2. The analysis of the optical absorption spectra is one of the most practical tools for understanding and developing the band structure and energy gap of semiconductor materials. The *effective band gap*, derived from the absorbance spectra, is by definition

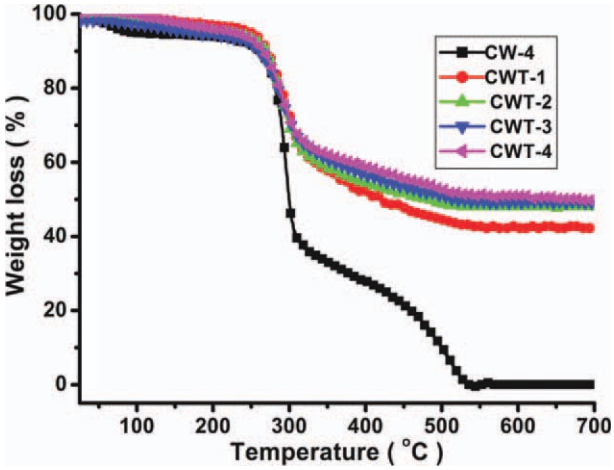

Figure 5 Weight loss (% of the initial weight) as a function of the temperature of the cellulose nanowhiskers and TiO_2/cellulose nanoparticles. [Color figure can be viewed in the online issue, which is available at wileyonlinelibrary.com.]

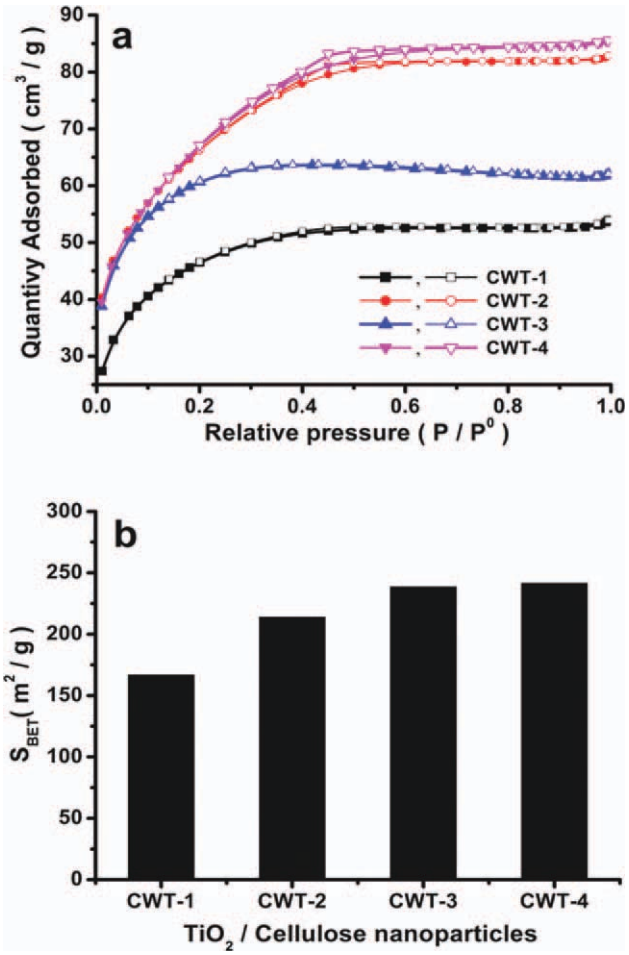

Figure 6 (a) Nitrogen gas adsorption–desorption isotherms and (b) corresponding BET surface areas (S_{BET}'s) of the TiO_2/cellulose nanoparticles (solid symbols indicate adsorption and open symbols indicate desorption). [Color figure can be viewed in the online issue, which is available at wileyonlinelibrary.com.]

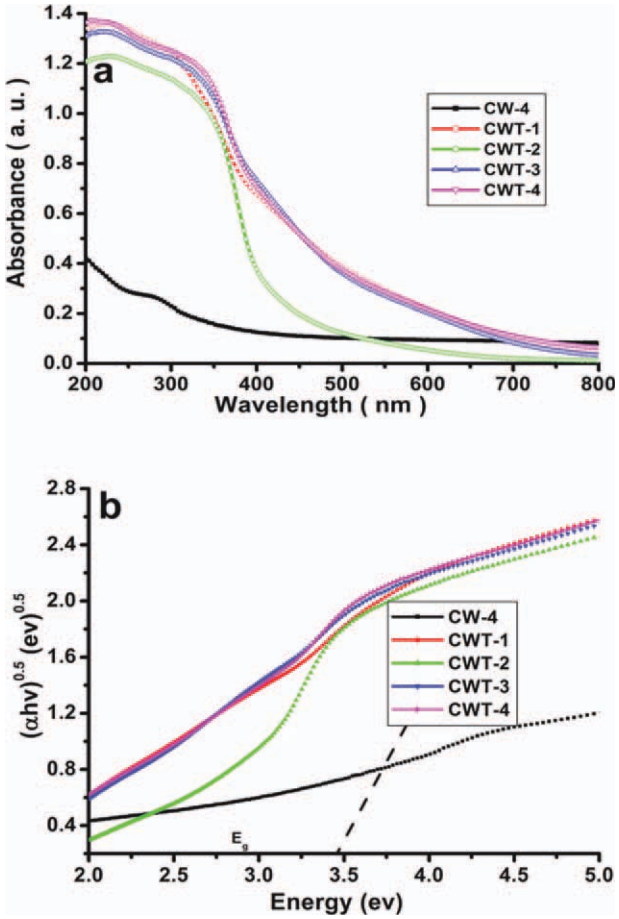

Figure 7 (a) UV–vis spectra of the TiO_2/cellulose nanoparticles made from cellulose crystals and (b) plot of $(\alpha h\nu)^{1/2}$ versus $h\nu$ for the indirect transition and E_g of the TiO_2/cellulose nanoparticles obtained by extrapolation to $\alpha = 0$. [Color figure can be viewed in the online issue, which is available at wileyonlinelibrary.com.]

the energy necessary to create an electron (e^-) and hole (h^+) pair. In principle, the excited electron–hole pair forms a bound state, that is, Wannier excitation, and the behavior of the excitation may be calculated with a confined excitation model, which gives an increase in the apparent band-gap energy. In semiconductor physics, the general expression that relates the absorption coefficient to the energy band gap is given by[47]

$$\alpha h\nu = k(h\nu - E_g)^n$$

where E_g is the optical band gap, $h\nu$ is the photoenergy, and k is a constant. In fact, α is the absorption coefficient (cm^{-1}), n is the index. n assumes values of $1/2$, $3/2$, 2, and 3 for allowed direct, forbidden direct, allowed indirect, and forbidden indirect transitions, respectively. Figure 7(b) plots the curves of $(\alpha h\nu)^{1/2}$ versus $h\nu$ for an allowed indirect transition with n equal to 2. The value of $h\nu$ extrapolated to $\alpha = 0$ gave the absorption band gap. The allowed

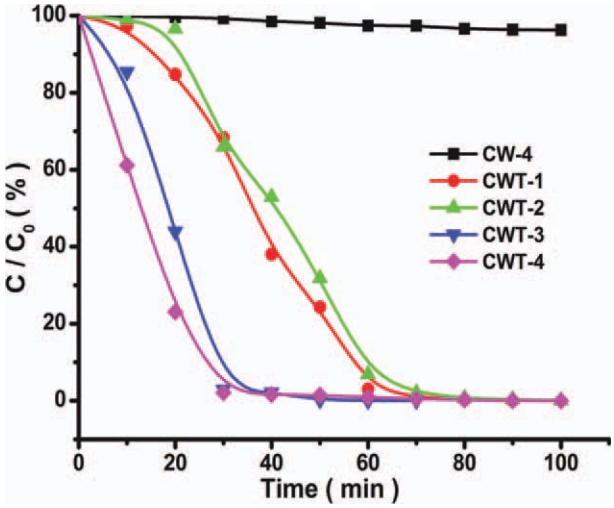

Figure 8 Process of the photocatalytic degradation of MO contained with cellulose nanowhiskers and different TiO_2/cellulose nanoparticles (40 mg) under UV light illumination (31.5 mW/cm^2). C was the concentration of MO at different degradation time, and C_o was the initial concentration of the MO. [Color figure can be viewed in the online issue, which is available at wileyonlinelibrary.com.]

indirect band-gap fit of the absorption edges gave a value of about 2.02 eV for the highest content and 2.74 eV for the lower content of loaded TiO_2 nanoparticles on the cellulose nanowhiskers. However, for the bulk anatase TiO_2, the band gap was about 3.18 ev[48], which was ascribed to the quantum size effect. The TiO_2 nanoparticles loaded on the surface of the cellulose nanocrystals had a fascinating photocatalytic activity.

The TiO_2/cellulose nanoparticles could degrade MO under UV light irradiation, as shown in Figure 8. The concentrations of the MO solutions containing

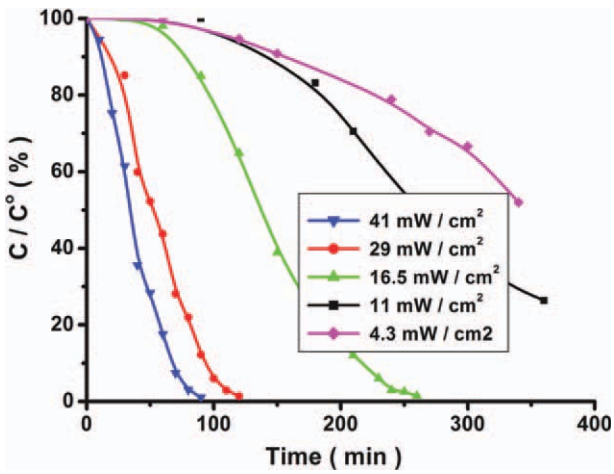

Figure 9 Effects of the UV intensity on the performance of CWT-4 (20 mg) for the photocatalytic degradation of MO. C was the concentration of MO at different degradation time, and C_o was the initial concentration of the MO. [Color figure can be viewed in the online issue, which is available at wileyonlinelibrary.com.]

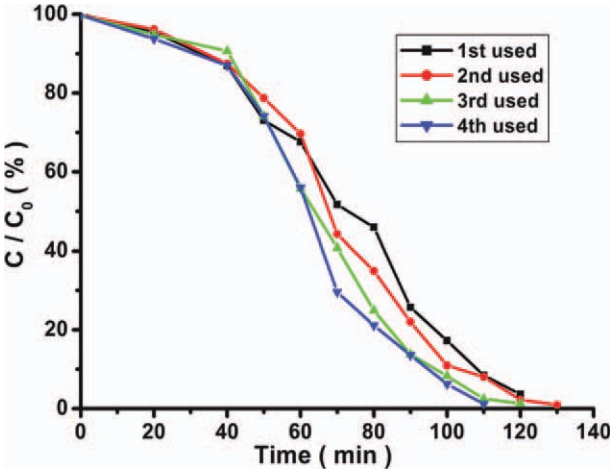

Figure 10 Cyclic photodegradation curves of MO with CWT-4 (20 mg) nanoparticles and a UV intensity of 38 mW/cm^2. C was the concentration of MO at different degradation time, and C_o was the initial concentration of the MO. [Color figure can be viewed in the online issue, which is available at wileyonlinelibrary.com.]

TiO_2/cellulose nanoparticles decreased gradually with increasing exposure time, whereas the concentration of the MO solution that contained pristine cellulose nanocrystals hardly changed. The MO solution could be photodegraded in 40 min with CWT-3 and CWT-4; this was faster than with CWT-1 and CWT-2 (60 min) and resulted from the fact that CWT-3 and CWT-4 had larger surface areas and higher TiO_2 loadings. The large surface area contributed to the high photocatalytic activity of the TiO_2 nanocrystals, where more reactive sites would have been created on the surface of the nanocomposites.[49] Moreover, the higher surface area of the nanocomposite particles would have favored the migration of photogenerated electrons and holes and led to the improvement of the photocatalytic activity. It is worth mentioning that the photocatalytic properties of the TiO_2/cellulose nanomaterials were attractive compared with those of the pure anatase TiO_2 nanoparticles.[50]

Usually, the intensity of UV light determines the time of photodegradation, and the time of photodegradation decreases with increasing UV light intensity. The photocatalytic activity of the CWT-4 nanoparticles under different intensities of UV light is shown in Figure 9. The degradation velocity of MO increased with increasing UV light intensity, and the TiO_2/cellulose nanoparticles exhibited good photocatalytic activity under weak UV light irradiation. Compared to the pure anatase TiO_2 photocatalyst, the use of cellulose nanocrystals as templates for the preparation of the TiO_2/cellulose nanowhiskers greatly reduced the amount of TiO_2, and the composite photocatalysts also had good photocatalytic abilities.

Photocatalytic stability of composite nanomaterials is very important for practical applications. The

cyclic photodegradation curves of CWT-4 under UV light irradiation are shown in Figure 10. CWT-4 exhibited a remarkable photostability without a loss of photocatalytic activity after repeated use. This suggested that the photocatalytic activity of the TiO_2/cellulose nanoparticles was very stable.[51] The immobilization of TiO_2 nanoparticles on the surface of the cellulose nanowhiskers endowed the TiO_2 nanoparticles with good stability against photocorrosion.[52] This is another prerequisite, as compared to TiO_2 nanoparticles, which always suffer from an instability problem.[53] The results succinctly demonstrate that the fabricated TiO_2/cellulose nanoparticles could be used as efficient photocatalysts for the degradation of organic pollutants.

CONCLUSIONS

Native cellulose nanocrystals were used as templates to assist in the preparation of 1 D TiO_2/cellulose nanoparticles. The particle size and morphology of cellulose nanocrystals could be controlled by changes in the hydrolysis time. Thus, the particle size and properties of the composite nanoparticles could also be controlled. The TiO_2/cellulose nanoparticles exhibited high photocatalytic activity in the degradation of MO with high concentration under weak UV light irradiation, and their photocatalytic efficiency was comparable to that of pure anatase TiO_2 nanoparticles. This approach for the fabrication of inorganic/organic nanocomposites or inorganic nanomaterials with native polymers as templates has many merits, including its simplicity, cost effectiveness, and versatility. This study provided a new conceptual scheme for the design and fabrication of functional nanomaterials, which could even open new application ranges for cellulose.

References

1. Joannopoulos, J. D.; Villeneuve, P. R.; Fan, S. Nature 1997, 386, 143.
2. Kawahara, T.; Konishi, Y.; Tada, H.; Tohge, N.; Nishii, J.; Ito, S. Angew Chem Int Ed 2002, 41, 2811.
3. Stark, W. J.; Wegner, K.; Pratsinis, S. E.; Baiker, A. J Catal 2001, 197, 182.
4. Oegan, B.; Gratzel, M. Nature 1991, 353, 737.
5. Kumazawa, N.; Islam, M. R.; Takeuchi, M. J Electroanal Chem 1999, 472, 137.
6. Kaune, G.; Haese-Seiller, M.; Kampmann, R.; Moulin, J.-F.; Zhong, Q.; Müller-Buschbaum, P. J Polym Sci Part B: Polym Phys 2010, 48, 1628.
7. Díaz-Visurraga, J.; Melendrez, M. F.; García, A.; Paulraj, M.; Cárdenas, G. J Appl Polym Sci 2010, 116, 3503.
8. Zhu, Y.; Shi, J.; Zhang, Z.; Zhang, C.; Zhang, X. Anal Chem 2002, 74, 120.
9. Hosseini, M. G.; Momeni, M. M.; Faraji, M. Electroanalysis 2010, 22, 2620.
10. Feldmann, C. Adv Mater 2001, 13, 1301.
11. Chu, S. Z.; Wada, K. J Phys Chem B 2003, 107, 10180.
12. Kim, C. S.; Moon, B. K.; Park, J. H.; Choi, B. C.; Seo, H. J. J Cryst Growth 2003, 257, 309.
13. Cozzoli, P. D.; Kornocoski, A.; Weller, H. J Am Chem Soc 2003, 125, 14539.
14. Jiang, X. C.; Wang, Y. L.; Herricks, T.; Xia, Y. N. J Mater Chem 2004, 14, 695.
15. Kolen'ko, Y. V.; Burukhin, A. A.; Churagulov, B. R.; Oleynikov, N. N. Mater Lett 2003, 57, 1124.
16. Kim, C. S.; Moon, B. K.; Park, J. H.; Chung, S. T.; Son, S. M. J Cryst Growth 2003, 254, 405.
17. Pradhan, S. K.; Reucroft, P. J.; Yang, F. Q.; Dozier, A. J Cryst Growth 2003, 56, 83.
18. Romano, S. D.; Kurlat, D. H. Chem Phys Lett 2000, 323, 93.
19. Li, X. L.; Peng, Q.; Yi, J. X.; Wang, X.; Li, Y. D. Chem—Eur J 2006, 12, 2383.
20. Xu, J.; Ge, J. P.; Li, Y. D. J Phys Chem B 2006, 110, 2497.
21. Wang, X.; Zhuang, J.; Peng, Q.; Li, Y. D. Nature 2005, 437, 121.
22. Zhao, L. X. Chem Mater 2001, 13, 2511.
23. Liu, S. M.; Gan, L. M.; Liu, L. H.; Zhang, W. D.; Zeng, H. C. Chem Mater 2002, 14, 1391.
24. Lei, Y.; Zhang, L. D.; Meng, G. W.; Li, G. H.; Zhang, X. Y.; Liang, C. H.; Cheng, W.; Wang, S. X. Appl Phys Lett 2001, 78, 1125.
25. Miao, Z.; Xu, D.; Ouyang, J.; Guo, G.; Zhao, X.; Tang, Y. Nano. Lett 2002, 2, 717.
26. Weng, C.-C.; Hsu, K.-F.; Wei, K.-H. Chem Mater 2004, 16, 4080.
27. Sturcova, A.; Davies, G. R.; Eichhorn, S. J. Biomacromolecules 2005, 6, 1055.
28. Dong, X. M.; Revol, J.-F.; Gray, D. G. Cellulose 1998, 5, 19.
29. Terech, P.; Chazeau, L.; Cavaille, J. Y. Macromolecules 1999, 32, 1872.
30. Hanley, S. J.; Giasson, J.; Revol, J.-F.;Gray. D. G. Polymer 1992, 33, 4639.
31. Grunert, M.; Winter, W. T. J Polym Environ 2002, 10, 27.
32. Beck-Candanedo, S.; Roman, M.; Gray, D. G. Biomacromolecules 2005, 6, 1048.
33. Liu, S.; Zhang, L.; Zhou, J.; Wu, R. J Phys Chem C 2008, 112, 4538.
34. Liu, S.; Zhou, J.; Zhang, L.; Guan, J.; Wang, J. Macromol Rapid Commun 2006, 27, 2084.
35. Luo, X.; Liu, S.; Zhou, J.; Zhang, L. J Mater Chem 2009, 19, 3538.
36. Ke, D.; Liu, S.; Dai, K.; Zhou, J.; Zhang, L.; Peng, T. J Phys Chem C 2009, 113, 16021.
37. Zeng, J.; Liu, S.; Cai, J.; Zhang, L. J Phys Chem C 2010, 114, 7806.
38. Liu, S.; Zhang, L.; Zhou, J.; Xiang, J.; Sun, J.; Guan, J Chem Mater 2008, 20, 3623.
39. Liu, S.; Zhang, L.; Zhou, J. J Phys Chem C 2011, 115, 3602.
40. Habibi, Y.; Lucia, L. A.; Rojas, O. J Chem Rev 2010, 110, 3479.
41. Michal, K.; Mietek, J Chem Mater 2001, 13, 3169.
42. Liu, H.; Zhang, L.; Seaton, N. A. J Colloid Interface Sci 1993, 156, 285.
43. Sayari, A.; Liu, P.; Kruk, M.; Jaroniec, M. Chem Mater 1997, 9, 2499.
44. Shin, Y.; Bae, I.-T.; Arey, B. W.; Exarhos, G. J. J Phys Chem B 2008, 112, 4844.
45. Liao, J.; Shi, L.; Yuan, S.; Zhao, Y.; Fang, J. J Phys Chem C 2009, 113, 18778.
46. Sing, K. S. W.; Everett, D. H.; Haul, R. A. W.; Moscou, L.; Pierotti, R. A.; Rouquerol, J.; Siemieniewska, T. Pure Appl Chem 1985, 57, 603.
47. Kim, G.-M.; Lee, S.-M.; Michler, G. H.; Roggendorf, H.; Gösele, U.; Knez, M. Chem Mater 2008, 20, 3085.
48. Serpone, N.; Lawless, D.; Khairutinou, R. J Phys Chem 1995, 99, 16646.
49. Liu, G.; Chen, Z. G.; Dong, C. L.; Zhao, Y. N.; Li, F.; Lu, G. Q.; Cheng, H. M. J Phys Chem B 2006, 110, 20823.
50. Chin, S.; Park, E.; Kim, M.; Bae, G.-N.; Jurng, J. J Colloid Interface Sci 2011, 362, 470.
51. Liu, Z.; Zhang, X.; Nishimoto, S.; Jin, M.; Tryk, D.; Murakami, T.; Fujishima, A. J Phys Chem C 2008, 112, 253.
52. Huang, J.; Kunitake, T. J Am Chem Soc 2003, 125, 11834.
53. Long, M.; Cai, W.; Cai, J.; Zhou, B.; Chai, X.; Wu, Y. J Phys Chem B 2006, 110, 20211.